SIXTH EUROPEAN ROTORCRAFT AND POWERED LIFT AIRCRAFT FORUM

Paper No. 30

WIND TUNNEL TESTS ON A CIRCULATION CONTROLLED AEROFOIL SECTION

N. J. Wood

J. F. Henderson

University of Bath
England

September 16-19, 1980
Bristol, England

WIND TUNNEL TESTS ON A CIRCULATION CONTROLLED AEROFOIL SECTION

N. J. Wood

J. F. Henderson

University of Bath, England

ABSTRACT

Two-dimensional subsonic wind tunnel tests have been conducted on a 20% thickness/chord ratio circulation controlled elliptic aerofoil section equipped with forward and reverse blowing slots. Overall performance measurements were made over a range of trailing edge blowing momentum coefficients from 0 to 0.04.

A detailed investigation of the trailing edge wall jet, using split film probes, hot wire probes and total head tubes, provided measurements of mean velocity components, Reynolds normal and shear stresses, and static pressure.

The results have led to suggestions regarding the nature of the flow field which should aid the theoretical solution of curved wall jet and Coanda flows.

NOTATION

C_L	lift coefficient, $\frac{\text{lift}}{\frac{1}{2}\rho U_\infty^2}$
C_μ	two-dimensional blowing momentum coefficient, $\frac{\dot{m} U_J}{\frac{1}{2}\rho U_\infty^2}$
$\dot{m}$	two-dimensional blowing jet mass flowrate
p	static pressure
p_∞	free stream static pressure
ρ	air density
R	radius of curvature of streamlines
R_o	local surface radius of curvature
U_∞	free stream velocity
U_J	nominal blowing jet velocity assuming uniform flow
U	mean velocity across wall jet
$\bar{U}$, $\bar{V}$	time averaged velocities tangential and normal to the surface at any point
$\bar{U}_m$	maximum velocity within the wall jet
$\frac{\sqrt{\overline{u'^2}}}{\bar{U}}$, $\frac{\sqrt{\overline{v'^2}}}{\bar{U}}$	longitudinal and normal turbulence intensities
$\overline{u'v'}$	Reynolds shear stress
y	distance normal to surface
$y_{m/2}$	distance at which average of maximum and edge-of-boundary-layer velocities occurs
α_G, α_{EFF}	geometric and effective incidences of aerofoil
θ	angular co-ordinate around trailing edge cylinder measured from slot position

1. INTRODUCTION

The advent of advanced technology applications of circulation control (X-wing[1] Kaman XH2/CCR[2]) demands a reliable performance prediction method for a variety of aerofoil sections. The key to this problem is the solution of the complex tangential wall jet flow around the bluff trailing edge typical of these aerofoils. Many attempts have been made to solve this Coanda flow, notably by Dvorak[3], Kind[4], Smith[5], but all have failed in some measure due to the large number of empirical constants needed in the theories and the small amount of useful experimental data on which to base their work. This leads to a position where each theory fits its own data but lacks universal application.

With this background it was decided to perform a series of detailed experiments on a circulation control aerofoil in order to provide a comprehensive set of reliable experimental data.

2. TEST AEROFOIL

The aerofoil section chosen was a 20% ellipse, with forward and reverse blowing slots located at 96.45% and 3.55% chord respectively (see Fig. 1).

The nominal chord was 24 in. with tangentially blended circular arc leading and trailing edges, giving a true chord of 23.425 in. (595 mm). The span was chosen as 27 in. (686 mm) to reduce production difficulties. The model was mounted vertically between endplates in the 7 ft wide x 5 ft high section of the wind tunnel to give the best available thickness and chord/tunnel 'height' ratio to reduce wall interference effects. There were 44 static pressure tappings around the aerofoil on the centreline.

The two blowing slots were identical and the slot gaps could be varied between 0.010 in and 0.045 in (0.25 mm and 1.14 mm). At the extreme spanwise locations of the trailing edge blowing slot, secondary blowing plenums were installed, ejecting through the main slot over a distance of 1 in. (25.4 mm). These "tip jets" (recommended by Ref. 6) provided control of the endplate boundary layers, and by blowing the tip jets in excess of the main slot, a significant reduction in three-dimensional effects was obtained.

Blowing momentum coefficients, C_μ, in the range 0 to 0.04 were used, the model being run at a test Reynolds number of 1.29×10^6 throughout.

The detailed investigation of the trailing edge wall jet was performed using single sensor hot wires, split films and flattened pitot tubes. These probes could all be mounted on a traversing gear located within the trailing edge cylinder, rotatable about the cylinder axis, with radial probe movement. A capacitance position control system was developed which gave repeatable positional accuracy of the probes, wind on or off, to better than 0.0005 in (0.013 mm)

3. TEST TECHNIQUES

3.1 Determination of effective incidence

Determination of the effective incidence, α_{EFF}, for circulation controlled aerofoils is complex and subject to error. Kind[4] used a method comparing predrawn potential flow pressure distributions with experiment. This permitted the downwash correction to be calculated and the effective incidence deduced. This method was adapted and improved in this study.

A CRT display at the wind tunnel console compared the measured pressure distribution with the potential flow solution, derived from the C_L of the leading half chord of the aerofoil, combined with an estimated effective incidence value. The operator then 'visually' iterated the potential flow solution to obtain the best fit to the observed pressure distribution over the leading half chord, by successive estimates of the effective incidence. The leading half chord was used to avoid the majority of the direct effects of the blowing jet.

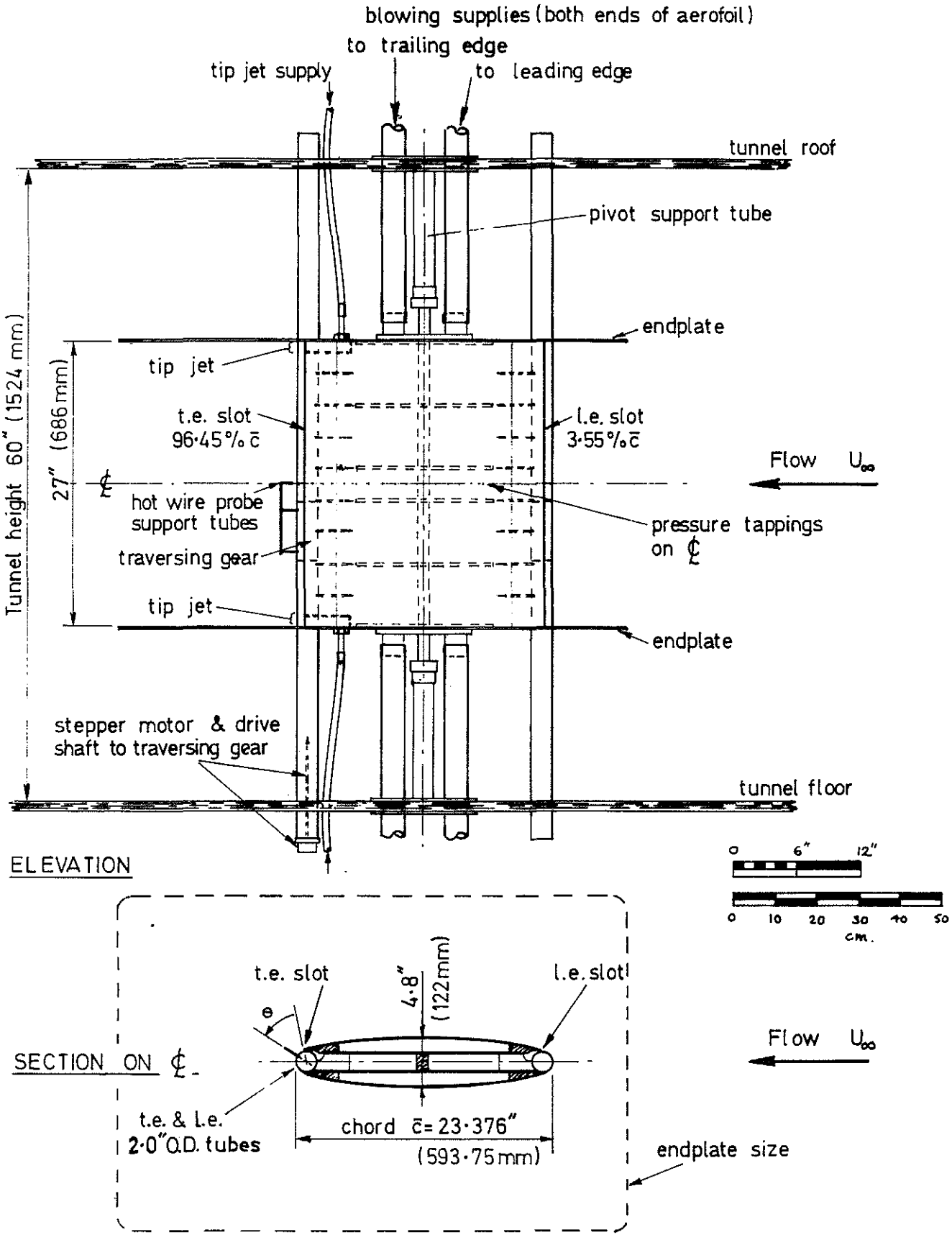

Fig. 1 General Arrangement of circulation controlled 20% elliptic aerofoil mounted in 7ft x 5ft wind tunnel

3.2 Anemometry

All hot wire/film probes were calibrated using a nozzle connected to the blowing supply, the mass flow being known from the calibrated orifice plate. Extensive investigations of the effects of temperature, flow angle and signal processing technique were performed and the necessary corrections applied[7].

3.2.1 Single wire anemometry

The single wires were operated from a DISA 55D01 anemometer at an overheat ratio of 0.8. The non-linearised results were processed by programmable pocket calculator to reduce computer time. The turbulence results were obtained using the method of Mojola[8].

Due to the cooling effect of the air supply pipework a temperature variation was present across the wall jet. This caused errors of up to 10% in the single wire results since the mean stagnation temperature was used in processing the anemometer output. Values of $\bar{U}$ and $\overline{u'^2}$ could be obtained to within 0.003 in (0.076 mm) of the surface and the upper limit of frequency response was found to be 40 kHz.

3.2.2 Split film probe

These relatively new probes were used as they offered a greatly improved spatial resolution compared with a standard dual sensor wire probe. Unfortunately, due to large thermal couplings of the probe, the bandwidth had to be limited to 10 KHz to avoid instabilities. The films were used with a Prosser twin channel anemometer system. The calibration was shown to be relatively insensitive to temperature, and the unlinearised results were processed digitally. Measurements of $\bar{U}$ were obtainable to within 0.009 in (0.229 mm) of the surface, while turbulence measurements were limited to within 0.035 in (0.89 mm) from the surface (approximately 7 probe diameters). The film probes showed excellent repeatability and satisfactory agreement with the wire probes.

3.3 Radial static pressure measurements

Many researchers of plane and curved wall jets had previously observed a static pressure difference across the flow[4,10,11] but none had measured, with any success, the distribution within the jet itself. The technique of Pache[9] offered advantages over conventional static pressure probes and was therefore used. A single wire sensor was aligned next to a flattened pitot tube (0.019 in (0.483 mm)) thick, and both were traversed radially through the wall jet. Account was taken of probe deflection, temperature, wall effects, density, shear flow and turbulence corrections. Precise measurements are difficult to make in these flows, but the authors feel that the present results indicate significant trends in the radial static pressure distribution.

4. RESULTS AND DISCUSSION

4.1 Tip jets

The effect of the tip jets is clearly shown in Fig. 2; the correct tip jet blowing pressure for two-dimensional flow was not immediately obvious. The technique adopted was to place a wool tuft at the junction of the tip and main jets and adjust the tip jet blowing pressure until the tuft was aligned parallel to the endplates.

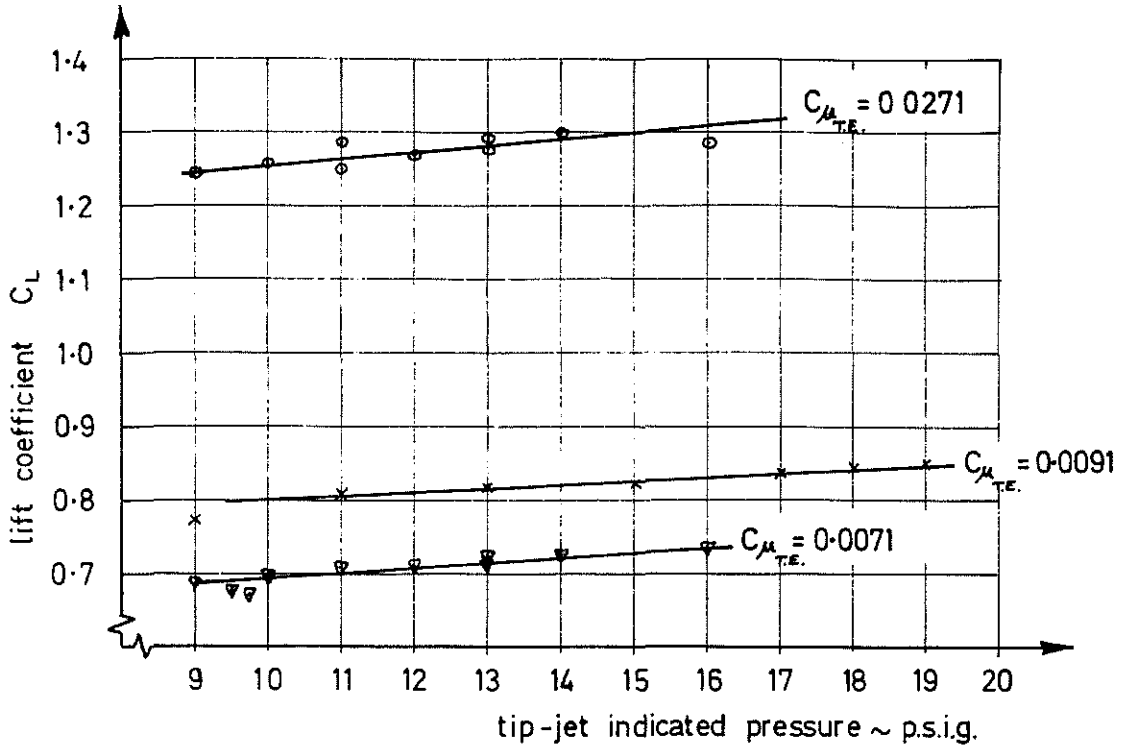

Fig. 2 Effects of tip jet blowing on lift coefficient (obtained from ℄ pressure tappings) at $\alpha_G = +5°$

4.2 Overall performance

The overall lift performance of the aerofoil shown in Fig.3 was as expected, and agreed well with other researchers.

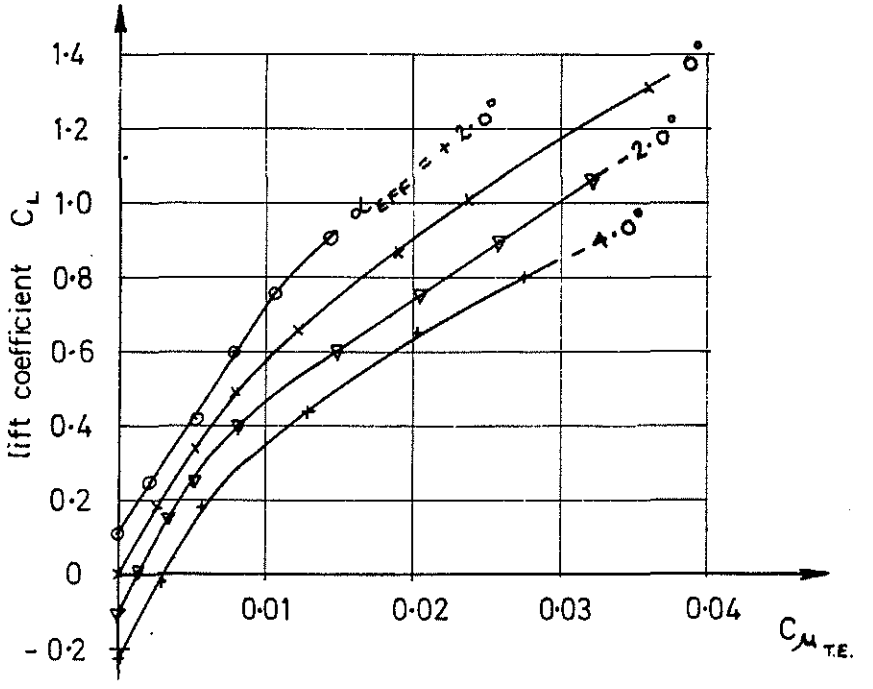

Fig. 3 Overall lift performance of aerofoil for constant values of $\alpha_{EFFECTIVE}$

4.3 Anemometer Results

4.3.1 Velocity profiles

Fig. 4 shows the velocity profiles obtained from the split film traverses,

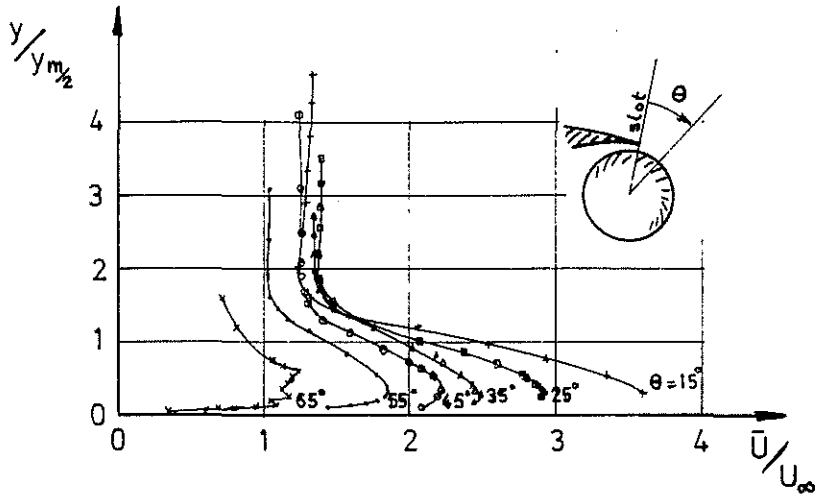

Fig. 4 Velocity profiles around the trailing edge cylinder downstream of the slot. $C_\mu = 0{\cdot}0284$, $\alpha_G = 0°$

and Fig. 5 shows the variation of $\bar{V}/\bar{U}$ (the local flow angle) against y and θ (angle from slot), also measured by the split film probe. The flow angle near the slot is of the order of 10° relative to the local surface.

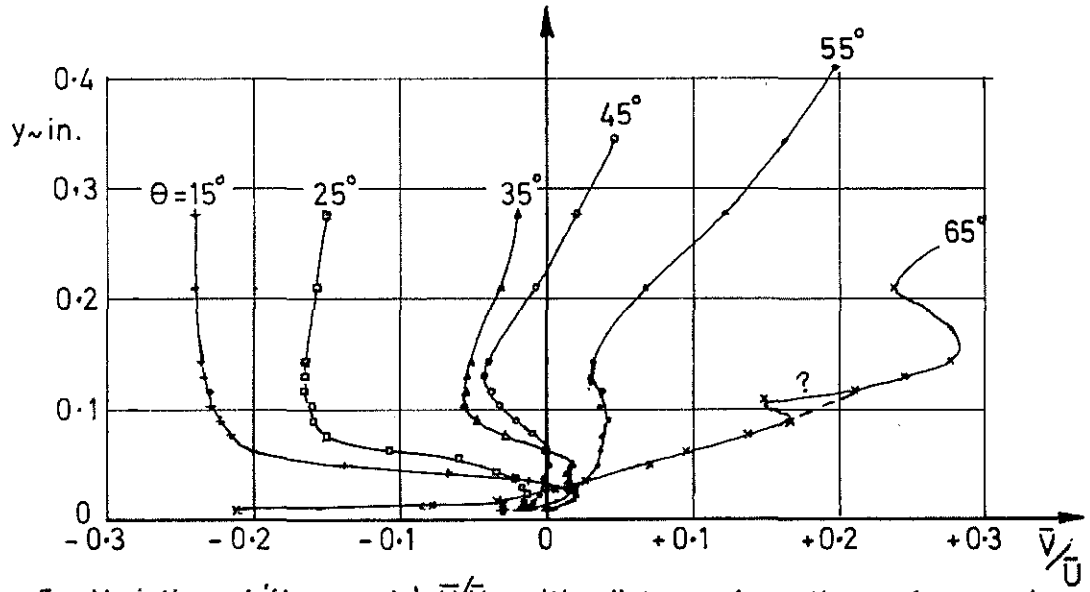

Fig. 5 Variation of 'flow angle' $\bar{V}/\bar{U}$ with distance from the surface and angular position downstream of the trailing edge slot. $C_{\mu_{TE}} = 0{\cdot}0284$, $\alpha_G = 0°$

4.3.2 Mean streamlines

The mean streamline patterns (Fig. 6) were derived from the velocity profiles. The entrainment of the upstream boundary layer, the growth of the wall jet and the wake of the slot lip are clearly indicated.

The radii of curvature of the streamlines were determined and are plotted in Fig. 7. They show that it is incorrect to assume streamlines concentric with the local surface centre of curvature, and that the radii can be nearly double the local surface radius.

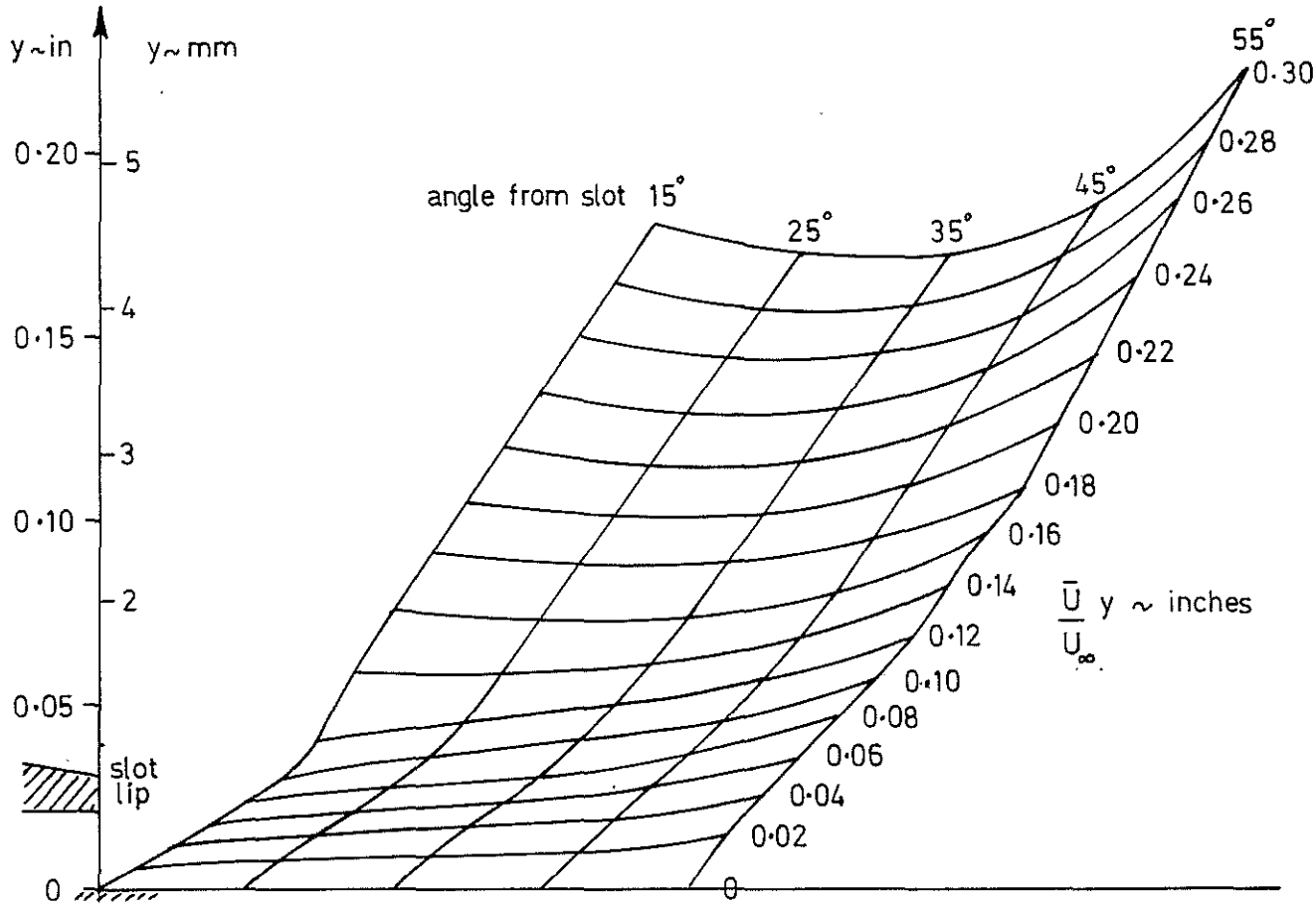

Fig. 6 Mean streamlines around trailing edge for $C_{\mu_{TE}} = 0{\cdot}0284$, $\alpha_G = 0°$

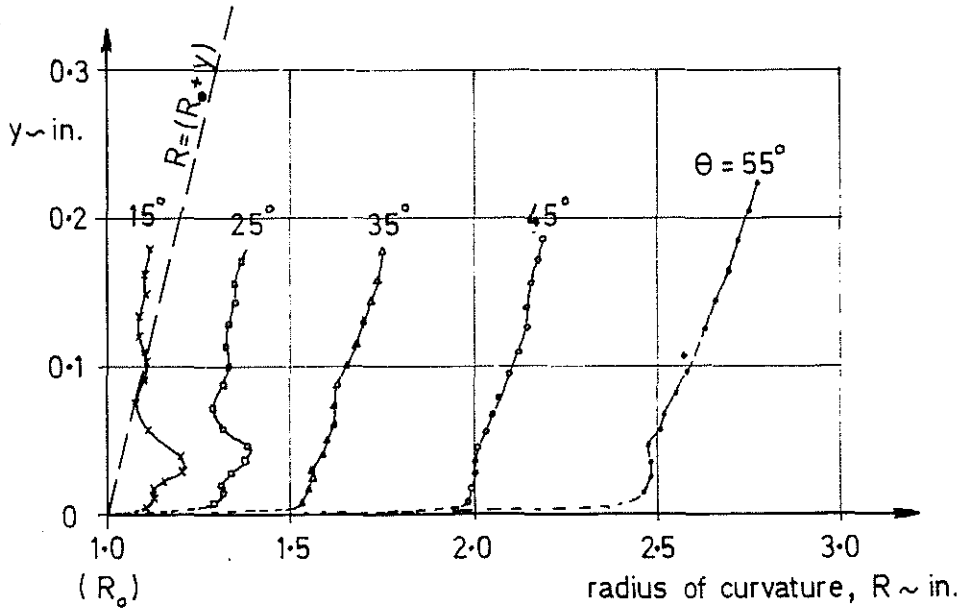

Fig. 7 Radius of curvature of mean streamlines around trailing edge $C_{\mu_{TE}} = 0{\cdot}0284$, $\alpha_G = 0°$

4.3.3 Turbulence parameters

4.3.3.1 Longitudinal turbulence intensity, $\sqrt{\overline{u'^2}}/\bar{U}$

Fig. 8 shows the longitudinal turbulence intensity derived from the split films and hot wires. The discrepancy between the wire and film results is due to the differing bandwidths of the two systems, although the position of $(\sqrt{\overline{u'^2}}/\bar{U})_{max}$ is repeated very accurately. The agreement between the film results and Kind[4] was excellent and suggests that the anemometer equipment used by Kind had a similar bandwidth. A simple sum based on a typical eddy size indicates that frequencies over 200 KHz may well exist in the wall jet flow.

4.3.3.2 Normal turbulence intensity, $\sqrt{\overline{v'^2}}/\bar{U}$

Fig. 9 shows the variation of $\overline{v'^2}$ across the jet, obtained from the split film probes. The results are not very revealing, indicating only that v'^2 follows a similar pattern to u'^2 but at about 60% of its intensity. It is assumed that v'^2 tends to zero at the wall and this is reflected by the increase of u'^2 adjacent to the wall as shown on the hot wire results in Fig. 8 .

4.3.3.3 Reynolds shear stress $\overline{u'v'}$

The shear stress distribution across the wall jet is shown in Fig. 10. Unfortunately, due to wall effects, the inner portion of the distribution has been lost. However, the results still indicate a non-zero value of $\overline{u'v'}$ at the velocity maximum.

4.3.3.4 General comments on turbulence parameters

It is interesting to note that all the turbulence parameters exhibit a minimum intensity shortly after the flow has stabilised, presumably caused by the change in sign of the longitudinal pressure gradient. It should also be noted that the turbulence $\sqrt{\overline{u'^2}}/\bar{U}$ measured by a hot wire close to the wall was seen to increase rapidly over that expected due to the suppression of $\sqrt{\overline{v'^2}}/\bar{U}$, as the flow developed. The authors suggest that this may be a 'pocket' of highly turbulent flow, possibly dependent on the surface roughness, which may act as a trigger for separation.

4.4 Radial static pressure

Fig. 11 shows the radial static pressure distribution measured around the trailing edge of the aerofoil. The first problem was to establish that these results were not being corrupted by turbulence or shear flow effects. The tests were repeated with different size pitot tubes, and many possible sources of error were examined, none of which, either singly or together had sufficient effect upon the distribution to remove their unexpected shape. Previous researchers, notably Englar[12], have investigated p(y) by other means, and their results are not totally dissimilar. For the current results the agreement with the value of the wall static pressure, obtained from the surface static pressure tappings is encouraging. It should also be noted that the overall radial pressure difference across the jet is in close agreement with the radial force balance

$$\frac{dp}{dy} = \frac{\rho U^2}{R}$$

where U is taken to be a mean value of the velocity across the jet.

Whilst the actual pressure differences are small, the pressure gradients are extremely large.

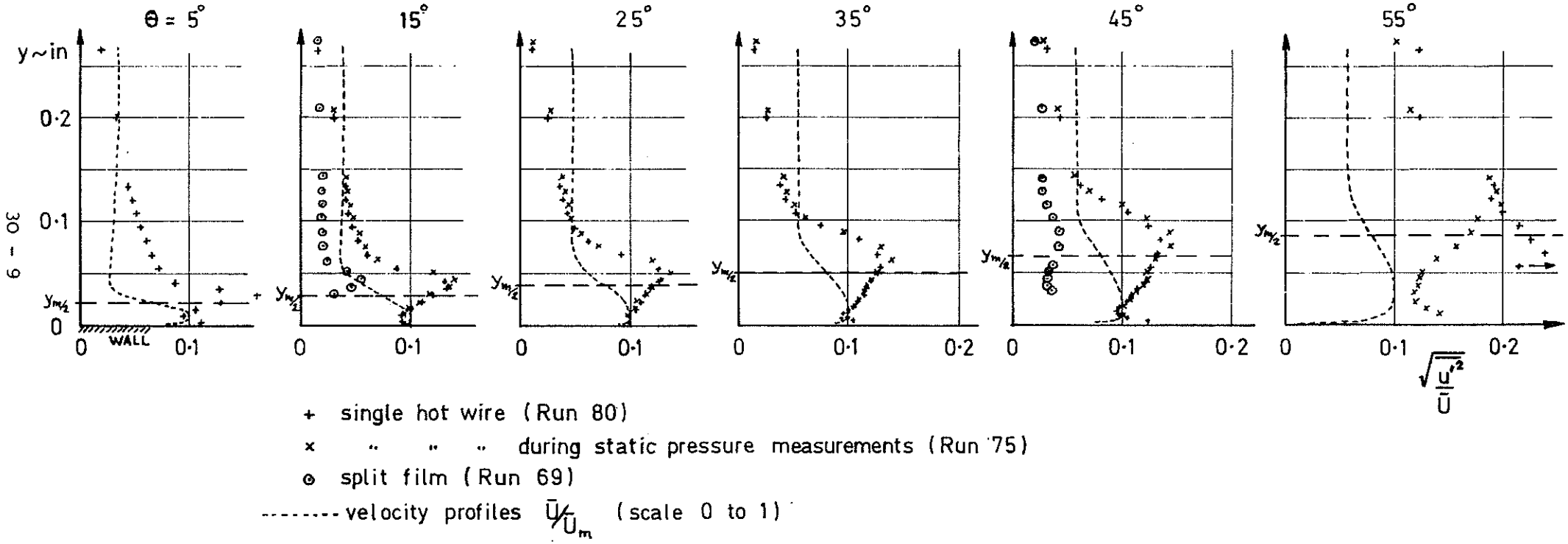

Fig. 8 Measurements of longitudinal turbulence intensity around trailing edge ($C_{\mu_{TE}} = 0{\cdot}0284$, $\alpha_G = 0°$) showing good repeatability of single wire results & effect of split film restricted bandwidth.

Velocity profiles are included for comparison

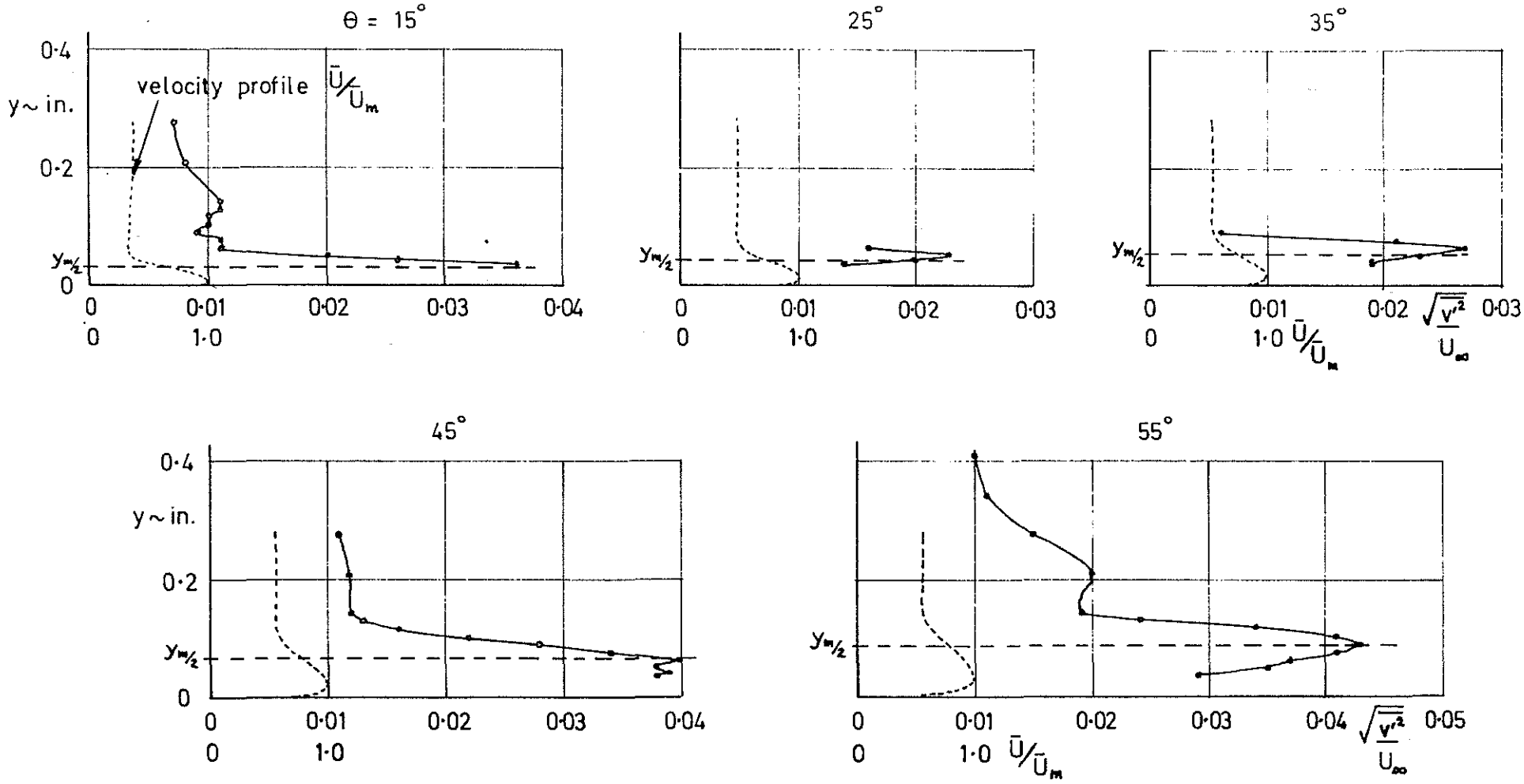

Fig. 9 Measurements of normal turbulence intensity around the trailing edge. Split film results at $C_{\mu_{TE}} = 0{\cdot}0284$, $\alpha_G = 0°$

Velocity profiles are included for comparison

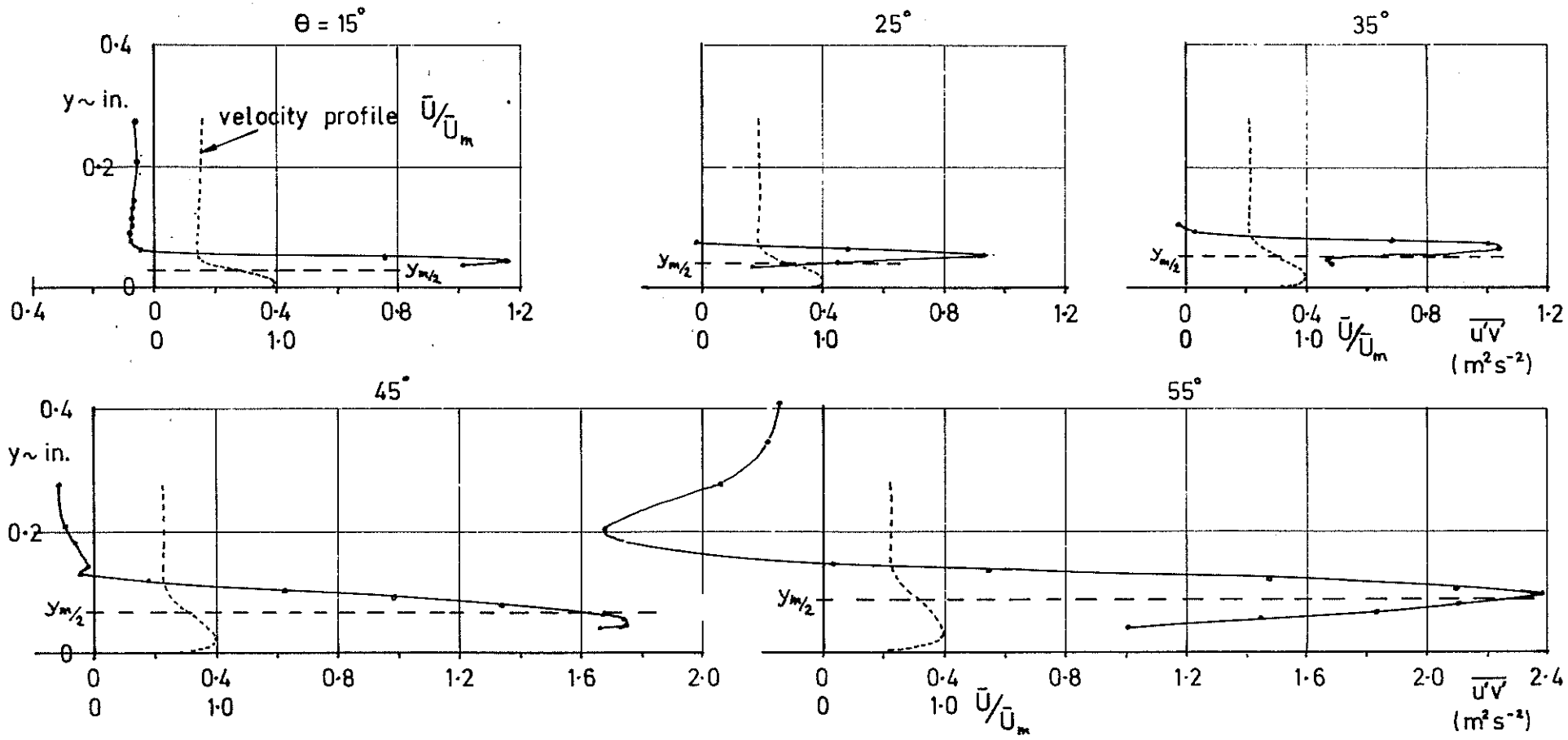

Fig. 10 Measurements of Reynolds shear stress $\overline{u'v'}$ around the trailing edge.
Split film results at $C_{\mu_{TE}} = 0{\cdot}0284$, $\alpha_G = 0°$

Velocity profiles are included for comparison

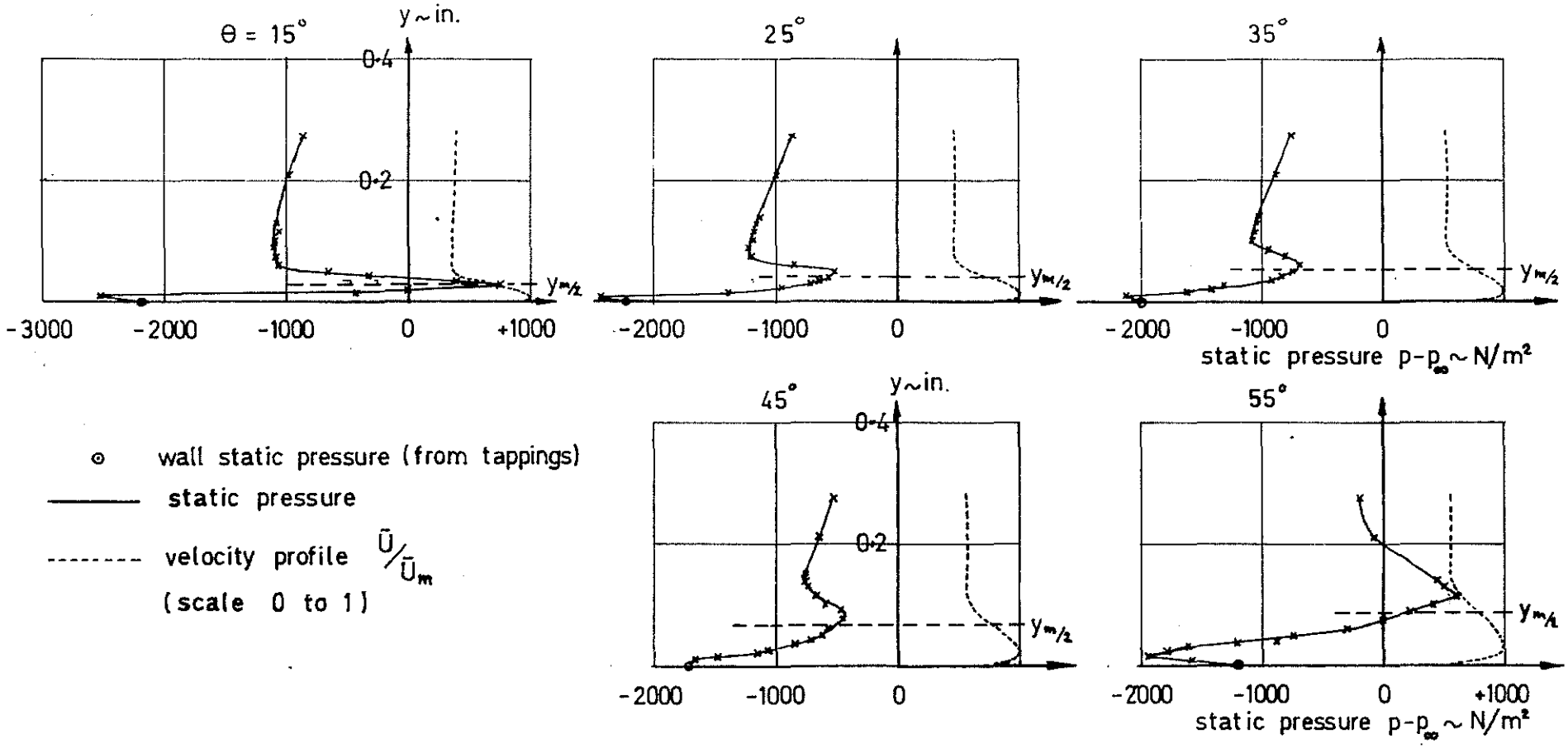

Fig. 11 Radial static pressure distributions measured in the wall jet around the trailing edge using Pache's method.[9] $C_{\mu_{TE}} = 0{\cdot}0284$, $\alpha_G = 0°$.

Velocity profiles are included for comparison.

Some possible physical justification is that the extreme inner negative gradient agrees with the hypothesis that close to the wall

$$\frac{1}{\rho}\frac{dp}{dy} \rightarrow -\frac{\partial(\overline{v'^2})}{\partial y}$$

The pressure gradient dp/dy then quickly takes a large positive value. Could it be that this is the reason why a Coanda flow remains attached?

At approximately $y\,m/_2$ (the mid-velocity point) the pressure gradient becomes negative, and remains so until just outside the minimum velocity point. Could this explain why a curved wall jet in the presence of an upstream boundary layer may split and form a detached separation bubble as reported by McGahon[13]? Outside the velocity minimum the pressure gradient again becomes positive; consistent with the required overall flow curvature around the trailing edge.

A further consideration is that perhaps the balance between the inner large positive and negative pressure gradients determines separation. It can be seen from Fig. 11 that, as separation is approached, the two inner gradients tend to equalise.

4.4.1 Balancing the equation

Since the experimental data gave values for each term in the angular momentum equation for curved flow

$$\frac{U}{y+R}\frac{\partial v}{\partial \theta} + v\frac{\partial v}{\partial y} - \frac{(U^2 + \overline{u'^2} - \overline{v'^2})}{y+R} = -\frac{\partial}{\partial y}\left(\frac{P}{\rho} + \overline{v'^2}\right) - \frac{1}{y+R}\frac{\partial}{\partial \theta}\,(\overline{u'\,v'})$$

these were inserted to see whether they would match the observed static pressure distribution. The pressure gradients produced from the equation were in some cases two orders of magnitude lower than those measured.

4.4.2 An observation on the hot wire anemometer signals

Fig. 12 shows an interesting observation of the hot wire anemometer signals - in sketch form as it could not be satisfactorily photographed. Near the velocity maximum the high pass filtered signal exhibited a positive bias, and near the velocity minimum a negative bias was indicated. This, coupled with the radial static pressure results, has led to some suggestions regarding the nature of the Coanda flow field.

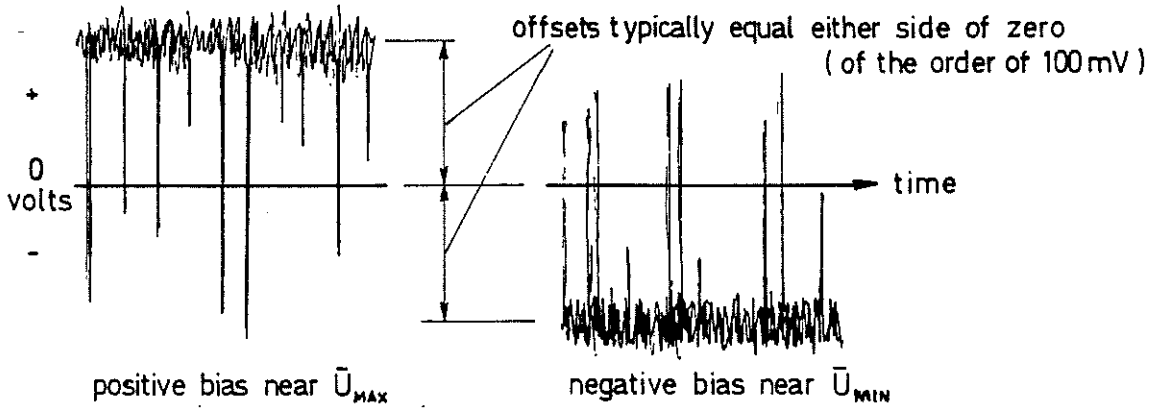

Fig. 12 Sketches of anemometer output signal observed during radial traverses with hot wire probe to obtain velocity profiles. High pass filter set at 2 Hz.

4.5 The Nature of the Coanda Wall Jet Flow Field

The suggested flow field is shown in Fig. 13 , and consists of a stream of coherent vortices being shed from the slot lip region. If the vortex cores are centred at roughly $y_{m/2}$, then the experimentally observed radial pressure distributions and velocity profiles should be obtained by a time averaging of the vortex field passing the sensing instruments.

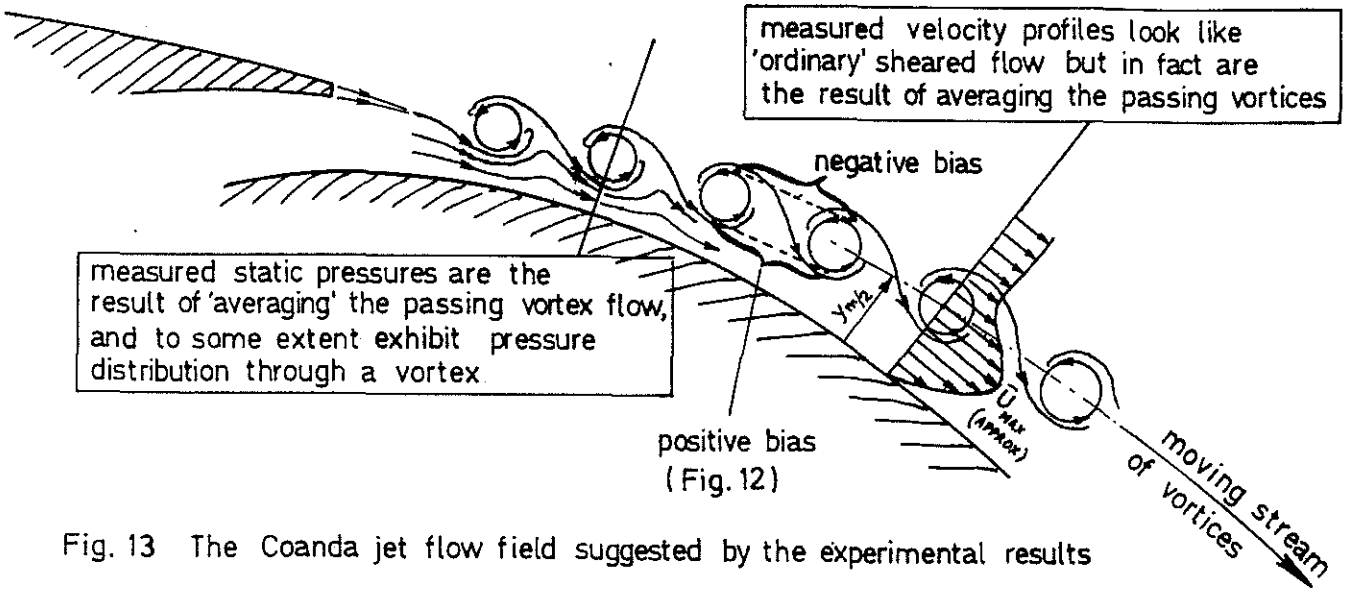

Fig. 13 The Coanda jet flow field suggested by the experimental results

The flow field is therefore consistent with the experimental results, and also explains the observations of Section 4.4.2 (Fig. 12) concerning the bias of the anemometer signals. The bias is just what would be expected from a stream of coherent vortices, and the 'turbulence' components are the result of the rapidly changing flow directions relative to the sensors as each vortex passes.

An unsuccessful attempt was made to determine the passing frequency of the vortex cores, their size and relative spacing, but an estimate of the possible streaming frequency suggests 40 - 60 KHz; right at the top of, and beyond, the anemometer frequency range.

Attention was drawn to vortex structures in the free shear layer of a plane wall jet by Clark & Markland[14], a report which seems to have been overlooked by researchers, and which has only recently come to our notice.

Similar effects are discussed by Davies[15] with reference to a free jet flow with similar jet/slot Reynolds numbers, and by Müller[16], in relation to noise generation. Evidence of radial static pressure gradients of similar nature to the current results has also been shown by Miller & Comings[17].

Damms & Küchemann[18] propose a similar flow field for predicting the mixing region between two parallel streams in the wake of a splitter plate. Their work is supported by experimental evidence, which suggests a core frequency of approximately 10 kHz at a streaming speed of roughly 35 ft/sec (11 m/sec).

In the light of this understanding of the flow field, the importance of slot and slot lip geometry become apparent, since the vortex formation near the slot lip may possibly be dependent on the values of dU/dy at the respective surfaces. ie. the external boundary layer and the slot duct boundary layer velocity profiles. This could explain the poor performance of some previous circulation control wind tunnel test specimens.

The splitting of the flow observed by McGahon[13] is perhaps the equivalent of vortex bursting.

If the flow field is as proposed, it could also explain why the many empirical theories based on solution of the Navier Stokes equations fail, since such an approach is inappropriate unless an inordinately fine mesh scale is used for the finite difference method. It suggests that perhaps the method of Smith[5] should be pursued for the Coanda flow region.

It is interesting to speculate on whether the leading edge jet flow can be solved theoretically by a similar flow model.

A more detailed appraisal of the flow field is in preparation in Ref. 7.

5. CONCLUSIONS

These tests strongly suggest that the flow field of the 'turbulent' wall jet Coanda flow is dominated by a moving stream of coherent vortices, and that it is the character of these vortices which is of primary importance in locating the flow separation point. The 'turbulence' observed in previous tests is largely the passage of the vortices at a frequency above the range of the anemometry equipment.

ACKNOWLEDGEMENTS

This work was supported by a Science Research Council Research Grant.

The authors thank Professor I. C. Cheeseman of the University of Southampton for his inspiration and encouragement; it was at a meeting with Professor Cheeseman that the nature of the flow field dawned on us collectively. We also thank Mr. R. M. Williams (NSRDC) for his interest, advice, assistance and enthusiasm.

We also gratefully acknowledge the technical staff of the University of Bath, especially Mr. H. Cox, Mr. T. Keston and Mr. J. Butt for their assistance in the building of the test facility.

REFERENCES

1. R. M. Williams — Application of circulation control rotor technology to a stopped rotor aircraft design. Presented at First European Rotorcraft and Powered Lift Aircraft Form, Southampton, Sept. 1975.

2. D. R. Barnes, D. G. Kirkpatrick, G. A. McCoubrey — Circulation control rotor flight demonstrator. Presented at American Helicopter Society Symposium on Rotor Technology, Aug. 1976.

3. F. A. Dvorak — A viscous/potential flow interaction analysis for circulation controlled airfoils. Analytical Methods Inc. Report 75.01.

4. R. J. Kind — A proposed method of circulation control. Ph.D. Thesis, Cambridge 1967.

5. R. V. Smith — A theoretical and experimental study of circulation control with reference to fixed wing applications. Ph.D. Thesis, Southampton 1978.

6. R. J. Englar, R. M. Williams — Test techniques for high lift two-dimensional airfoils with boundary layer and circulation control for application to rotary wing aircraft. N.S.R.D.C. Report 4645, Jul 1975.

7. N. J. Wood — The aerodynamics of circulation controlled aerofoils. Ph.D. Thesis in preparation, University of Bath.

8. O. O. Mojola — A hot-wire method for three-dimensional shear flows. DISA Information No. 16, Jul 1974 (pp. 11-14).

9. W. Pache — Measuring the mean static pressure in turbulent or high frequency fluctuating flow. DISA Information No. 22, Dec 1977 (pp. 29-33).

10. S. C. Kacker, J. H. Whitelaw — Some properties of the two-dimensional turbulent wall jet in a moving stream. J. Applied Mechanics, Dec 1968 (pp. 641-651).

11. V. Kruka, S. Eskinazi — The wall jet in a moving stream. J. Fluid Mechanics 1964, Vol. 20, pt. 4 (pp. 555-579).

12. R. J. Englar — Experimental investigation of the high velocity Coanda wall jet applied to bluff trailing edge circulation control airfoils. N.S.R.D.C. Report 4708 Sep 1975.

13. W. A. McGahon — The incompressible turbulent wall jet in an adverse pressure gradient. Ph.D. Thesis M.I.T. 1965.

14. J. A. Clark, E. Markland — Vortex structures in the free shear layer of a plane wall jet. Queen's University Belfast, Dept. Mech. Eng. Report 471, 1970.

15. P. O. A. L. Davies, D. R. J. Baxter — Transition in free shear layers. Institute of Sound & Vibration Research. Southampton University.

16. E. A. Müller — Mechanics of sound generation in flows. AIAA Symposium, Göttingen, Aug 1979.

17. D. R. Miller, E. W. Comings — Static pressure in the free turbulent jet. J. Fluid Mech. Vol. 3, Part 1, Oct 1957.

18. S. M. Damms, D. Küchemann — On a vortex-sheet model for the mixing between two parallel streams. RAE Tech. Report 72139, Aug 1972.